Title

Free Extracellular Diffusion Creates the Dpp Morphogen Gradient of the Drosophila Wing Disc

Journal

Current Biology, 22(8)

ISSN

0960-9822

Authors

Zhou, Shaohua
Lo, Wing-Cheong
Suhalim, Jeffrey L
et al.

Publication Date

2012-04-01

DOI

10.1016/j.cub.2012.02.065

Published in final edited form as:
Curr Biol. 2012 April 24; 22(8): 668–675. doi:10.1016/j.cub.2012.02.065.

Free Extracellular Diffusion Creates the Dpp Morphogen Gradient of the *Drosophila* Wing Disc

Shaohua Zhou[1,4], **Wing-Cheong Lo**[2,4], **Jeffrey Suhalim**[1,4], **Michelle A Digman**[3,4,5], **Enrico Gratton**[3,4,5], **Qing Nie**[2,3,4], and **Arthur D. Lander**[1,3,4,*]

[1]Department of Developmental and Cell Biology, University of California, Irvine, CA 92697, USA

[2]Department of Mathematics, University of California, Irvine, CA 92697, USA

[3]Department of Biomedical Engineering, University of California, Irvine, CA 92697, USA

[4]Center for Complex Biological Systems, University of California, Irvine, CA 92697, USA

[5]Laboratory for Fluorescence Dynamics, University of California, Irvine, CA 92697, USA

SUMMARY

Background—How morphogen gradients form has long been a subject of controversy. The strongest support for the view that morphogens do not simply spread by free diffusion has come from a variety of studies of the Decapentaplegic (Dpp) gradient of the *Drosophila* larval wing disc.

Results—In the present study, we initially show how the failure, in such studies, to consider the coupling of transport to receptor-mediated uptake and degradation has led to estimates of transport rates that are orders of magnitude too low, lending unwarranted support to a variety of hypothetical mechanisms, such as “planar transcytosis” and “restricted extracellular diffusion”. Using several independent dynamic methods, we obtain data that are inconsistent with such models, and that show directly that Dpp transport occurs by simple, rapid diffusion in the extracellular space. We discuss the implications of these findings for other morphogen systems in which complex transport mechanisms have been proposed.

Conclusions—We believe that these findings resolve a major, longstanding question about morphogen gradient formation, and provide a solid framework for interpreting experimental observations of morphogen gradient dynamics.

INTRODUCTION

Biological pattern formation is often orchestrated by morphogens, molecules that, when released at discrete locations, form concentration gradients from which cells obtain positional information. The idea that such gradients form by simple diffusion was advocated by Crick, based on observed constraints on gradient sizes [1], and many quantitative models

*Author for Correspondence Department of Developmental and Cell Biology, 2638 Bio Sci III, University of California, Irvine, Irvine, CA 92697-2300, Tel: 949-824-1721, Fax: 949-824-4709, adlander@uci.edu.

Supporting Online Material
Figs. S1–S9
Mathematical Analysis and Modeling

of morphogen gradients assume this mechanism [e.g. 2, 3–7]. It has been argued, however, that some experimental results are inconsistent with diffusive transport of extracellular morphogens [8–11], and theoretical objections have been raised against free diffusion for not being sufficiently robust [12] or controllable [13].

Attempts to resolve this controversy by following the behaviors of fluorescently-tagged morphogens have yielded conflicting results. In the *Drosophila* larval wing imaginal disc, studies with labeled Decapentaplegic (DppGFP) suggested a transport coefficient of 0.1 μm^2 sec^{-1}, two orders of magnitude too slow for free diffusion [9]. Such measurements lend support to the view that morphogens move by active mechanisms such as serial transcytosis (i.e., repeated rounds of endo- and exocytosis [12]), travel along or within specialized filopodia, [14, 15], or by "restricted" diffusion, in which transport involves transfers between immobile sites in the extracellular matrix [16]. In contrast, in the zebrafish neural tube, studies of fluorescently-tagged fibroblast growth factor 8 (Fgf8) have yielded much faster transport rates, (D=50–90 μm^2 sec^{-1}), consistent with simple, free diffusion in the extracellular space [17]. With the cytoplasmic morphogen Bicoid, which forms a gradient in the syncytial *Drosophila* embryo, different approaches have led to estimates of transport coefficients ranging from as low as 0.3 to as high as 7 μm^2 sec^{-1} [18–20].

Although it has been suggested that different morphogens move by different mechanisms, or that different transport processes operate over short versus long distances [17, 19, 21, 22], we wondered whether some of the perceived variability in morphogen transport behavior might reflect the misinterpretation of data, and not real biological differences. Here we present evidence in support of this view, based upon observations and analysis of the Dpp gradient of the *Drosophila* wing disc. We believe this work lays to rest long-standing controversies about Dpp transport, and suggests ways in which to guide future inquiry into the transport of morphogens in general.

RESULTS

We note that most reports claiming to provide strong evidence for morphogen transport at rates much slower than free diffusion have utilized the method of fluorescence recovery after photobleaching (FRAP). For example, Kicheva et al., [9] and Gregor et al., [18] used the kinetics of FRAP—i.e. the rate of recovery of a photobleached zone—to estimate spreading rates for DppGFP and BicoidGFP, as 0.1 μm^2 sec^{-1}, and 0.3 μm^2 sec^{-1} respectively. Typically, when deriving transport rates from FRAP kinetics, one assumes that transport is the only process upon which accumulation of observed molecules during the observation time depends. This assumption is often not stated explicitly, but is critical: If other processes, such as binding to immobile sites, or degradation, occur on the time scale of observation, FRAP kinetics can be dominated by these processes, and may contain little information about transport. Although an extended treatment of this issue is provided elsewhere (see SI, "Mathematical analysis and modeling"), a simple illustration makes the point: Here we consider two mathematical models of morphogen gradient formation in a *Drosophila* wing disc. In one, transport occurs by an inherently slow process (e.g. transcytosis), at the rate reported by Kicheva et al. [9], i.e. D=0.1 μm^2 sec^{-1}. In the other, morphogen molecules move by fast, unhindered, extracellular diffusion (D=20 μm^2 sec^{-1}), but are subjected to receptor-mediated uptake, internalization and degradation (using rate constants consistent with the Dpp gradient length-scale normally observed in late larval wing discs [23]).

Figure 1 shows the expected kinetics of recovery after photobleaching, according to the two models. Despite having transport rates 200-fold apart, they predict nearly indistinguishable FRAP behavior. The reason is that, in the model that assumes slow transport, FRAP kinetics

are dominated by the transport rate, whereas in the model that assumes fast, diffusive transport, the kinetics are dominated by the morphogen degradation rate, and are essentially independent of transport. Thus, one cannot derive a transport rate from a FRAP experiment of the type shown, unless one has already assumed *a priori* that transport is not fast. Generally speaking, situations in which FRAP kinetics will fail to provide useful information about transport rate are those in which two conditions are met: Transport is fast relative to the time- and length-scale of observation; and degradation is sufficiently slow that, at steady state, the amount of morphogen accumulated on and within cells is much larger than the amount freely diffusing in the extracellular space.

Are these conditions met by Dpp in the wing disc? Calculations suggest they easily could be. First, if Dpp were to move by free diffusion ($D \geq 10\ \mu m^2\ sec^{-1}$), one would expect it to traverse distances of ~30 μm (the typical maximum distance over which FRAP is performed in the wing disc) in ≤ 20 sec, much shorter than typical FRAP observation times (tens of minutes). Second, from fluorescent images it has been estimated that >85% of the Dpp in wing discs is inside cells [9, 24]. Of the remainder, the amount free in the extracellular space (as opposed to being bound to cell-surface molecules) cannot be determined from images, but may be estimated, given recent measurements of absolute DppGFP concentrations (~800 molecules/μm^2 near the Dpp source [9]); estimates of the extracellular volume fraction [2]; and the reasonable assumption that free extracellular Dpp does not greatly exceed the effective dissociation constant of its receptor (see SI). Based on this information one can calculate that free extracellular Dpp is unlikely to account for more than 3% of the total morphogen, and less than 1% of that which is normally visualized by fluorescence imaging (see SI; note that this calculation makes no assumptions about transport mechanisms).

It may seem counterintuitive that the free diffusion of such a small fraction of total morphogen can support the formation of the entire Dpp gradient, but it is precisely when diffusion is fast that this is so. In effect, a scarcity of extracellular Dpp, rather than arguing against transport by diffusion, as others have suggested [9], is just what free diffusive transport predicts (see SI, section 1.2).

How then might one determine, experimentally, whether morphogen transport occurs by free diffusion, or some slow process such as transcytosis or “restricted” diffusion? Here we apply four approaches to the Dpp gradient of the wing disc: fluorescence spreading after photoactivation, spatial FRAP, FCS, and pair correlation function microscopy. In each case, the results support transport by free, extracellular diffusion.

Photoactivation relies upon the ability to tag molecules with probes that can be rendered abruptly fluorescent with brief pulses of light, and has been used as a means to follow proteins within cells [25]. We fused Dpp to Dendra2, which switches from green fluorescence to red after exposure to UV light [26], and expressed it in the normal Dpp expression domain of the wing disc. DppDendra2 formed gradients along the anteroposterior axis similar to those observed with Dpp tagged with GFP [8, 24] or other moieties [27]; it also turned on Dpp target genes at appropriate locations (Fig. S1 and Methods and Materials). Like DppGFP [8, 9, 24], DppDendra2 was mainly found in punctuate intracellular accumulations in the most apical 5 μm of the columnar disc epithelial cells. We carried out FRAP experiments with DppDendra2, and obtained results similar to those reported for DppGFP [9]: recovery on a timescale of 10–15 min, and a large “immobile fraction” (non- or very slowly-recovering fraction; Fig. S1).

Thus, in all regards tested, DppDendra2 behaved like other tagged forms of Dpp in the wing disc. Yet when regions within the DppDendra2 gradient were photoactivated and followed, no obvious spreading of red fluorescence was seen. To increase the ability to detect

spreading, we photoactivated pairs of stripes 10 μm apart, and looked in the region between them; still no significant spreading was evident, either on short or long time scales (minutes to hours; Figure 2A-O, Fig. S2A-B). To further improve sensitivity, we pre-bleached a large region within the DppDendra2 gradient, waited 30 min for fluorescence recovery, then photoactivated within this region (pre-bleaching removes background fluorescence due to "immobile fractions"). Even then, fluorescence spreading after photoactivation was undetectable (Fig. S2). To control for the possibility that background autofluorescence, fluctuating laser power, sample movement, or other such artifacts might mask small amounts of spreading, we also followed the intracellular puncta of photoactivated DppDendra2 at high magnification, and observed no obvious increases in the numbers or sizes of such accumulations next to photoactivated regions over a 30 minute interval (Fig. S2).

The explanation for these results cannot be that fusion to Dendra2 prevents Dpp transport, since DppDendra2 molecules formed a normal morphogen gradient, and behaved similarly to DppGFP in FRAP studies (Fig. S1). It also seemed unlikely that photoactivation *per se* interfered with the transport of DppDendra2 molecules, given the relatively low energy of laser light used. However, to control for this possibility, we fused Dendra2 to another morphogen, Wingless. When expressed and photoactivated in the wing disc, spreading of a significant fraction of Wg-Dendra2 fluorescence was observed (Fig. 2P-Z).

The lack of detectable spreading of photoactivated Dpp is predicted by models of transport by free extracellular diffusion because, in such models, only a small fraction of total Dpp participates in transport; the vast majority is trapped permanently on or within cells. In contrast, under the model of transport by transcytosis, 30% of total Dpp must be moving from cell to cell to fit FRAP data (this rises to 60–70% in the case of a freshly-recovered pre-bleached region, as in Fig. S2). Under such conditions, spreading after photoactivation should be quite obvious, peaking at ~5 min after photoactivation (see SI). Note that similar predictions are also made by the "restricted extracellular diffusion" model, as it is the slow rate of transport *per se*, and not the particular model, that necessitates such behavior (see SI).

As a second approach for assessing the means of Dpp transport, we used "spatial FRAP", in which fluorescence recovery is followed as a function of location within a photobleached region. Even when overall FRAP kinetics are dominated by processes other than transport, differences in recovery times at different distances from a bleach-boundary can potentially provide a measure of transport rate (see SI, "Mathematical Analysis and Modeling"). Kicheva et al., [9] presented, as supplemental data, several spatial FRAP experiments for DppGFP in the wing disc, and fit the results to the predictions of a transcytosis model. However, their experiments were not designed to distinguish among transport models, and in most cases, were carried out using geometries in which both fast (e.g. free extracellular diffusion) and slow (e.g. transcytosis or restricted diffusion) models could still fit the data. The optimal configuration for distinguishing among models is one in which two sites are observed, such that fluorescence recovery at one requires prior transport through the other. This can be achieved by bleaching a large rectangle, and comparing recovery in its center with recovery in the rectangle as a whole. When we did this with DppDendra2-expressing wing discs, the lack of significant delay in central recovery (Fig. 3) implied a rate of transport far faster than 0.1 $\mu m^2\ sec^{-1}$.

If such fast transport is truly due to free extracellular diffusion, we ought, in principle, to be able to observe it directly. Although freely diffusing Dpp molecules are expected to be rare (on the order of 8 molecules or less per μm^2, given the calculations mentioned previously), their existence should be detectable by FCS, which is effectively a single-molecule method. FCS uses fluctuations in signal intensity to measure average residency times of fluorescent

molecules within a small (~1 fL) volume illuminated by a laser beam. Because intercellular spaces in the wing disc are too narrow to resolve by light microscopy, we labeled plasma membranes with the vital dye FM4-64, and used its fluorescence to focus the laser at sites of cell-cell contact (Fig. 4A).

When FCS was performed on discs expressing DppDendra2, the data were well fit by a two-species model, in which 65% of the autocorrelation signal comes from molecules that diffuse rapidly (D=21 ± 3 μm^2 s^{-1}), and 35% from ones that move much more slowly (D=0.03 ± 0.006 μm^2 s^{-1}) (green triangles in Fig. 4B). Similar results were obtained in discs expressing DppGFP (Fig. 4C,D). The fast diffusion coefficients obtained in these experiments are appropriate for a freely soluble protein in extracellular space. The slower diffusion coefficients are consistent with Dpp bound to proteins of the plasma membrane (e.g. receptors, glypicans [27, 28]). Interestingly, when FCS experiments were repeated in discs mutant for the glypican dally, which has been suggested to play a major role in shaping the Dpp gradient [11, 27, 28], we observed only a small change in the relative contributions of fast and slow moving species (Fig. S3), suggesting that the slowly moving pool is not primarily composed of dally-bound Dpp. As a negative control, we also expressed a GFP-tagged transmembrane protein, cd8, in the wing disc, and measured its diffusivity. Consistent with expectations for an integral membrane protein, only a single, slow diffusion coefficient was observed (0.05 ± 0.003 μm^2 s^{-1}; grey crosses in Fig. 4B).

The calculation of transport parameters from FCS depends upon assumptions that can be difficult to validate in complex tissues (e.g., knowledge of the size and shape of the illuminated volume). To measure diffusivity independent of such assumptions, we also used a new method, Pair Correlation Function (pCF) microscopy [29–31]. In pCF, fluorescence is followed at two points. The time required for fluctuations at one point to arrive at the other provides a direct measure of transport rate, independent of the details of the fluctuations themselves. Fig. 4E-G shows the results of pCF, in a DppDendra2-expressing wing disc, in which the points were 5 pixels apart, along a border between two cells. Cross-correlation demonstrated the existence of a population of fluorescent molecules that take 5.1 ± 1.1 ms to traverse 0.525 μm. This corresponds to an effective diffusion coefficient of 21 ± 4 μm^2 sec^{-1}, essentially identical to the one measured by FCS (Fig. 4D). As evidence that such cross-correlations truly represent transport, when observations were made at one point on a border between two cells and a second point inside one of the cells, positive cross-correlation was not seen (Fig. S4).

DISCUSSION

The results described above strongly support the view that the Dpp gradient of the *Drosophila* wing disc forms by free, extracellular diffusion, coupled with uptake by cell-surface receptors, and subsequent degradation. It is precisely because transport is fast, relative to uptake and degradation, that fluorescence recovery kinetics in a simple FRAP experiment fail to provide information about transport. It is also precisely because transport is fast that very little Dpp needs to be in the transported pool (i.e. free in the extracellular space). Indeed, in the wing disc, Dpp molecules actually undergoing transport may be sufficiently rare that only methods with single-molecule sensitivity, such as FCS and pCF microscopy, can reliably detect them.

Although the experimental data presented here focus on the Dpp gradient of the wing disc, other morphogen systems likely face similar issues. For example, the fact that measurements of Bicoid transport in the early *Drosophila* embryo by FRAP [18, 20] yield values 8–23 times smaller than measurements by FCS [19], could be explained by reversible binding of Bicoid to immobile structures (e.g. cytoskeletal components, organelles). FRAP kinetics

might then reflect the dissociation rate from such structures, rather than Bicoid transport (see SI).

Recently, Schwank et al. [16] used genetic manipulations to show that the spread of Dpp in the wing disc does not require its receptor, thickveins (Tkv), thereby arguing against transport through receptor-mediated transcytosis. Although they acknowledged that such data do not rule out other forms of transcytosis, they favored a “restricted extracellular diffusion” model, in which Dpp transport occurs through periodic binding and unbinding from immobile sites in the extracellular matrix. In support of this, they cited the slow Dpp transport kinetics inferred by Kicheva et al. [9], but as we have seen here, those data only imply slow transport if one has already assumed that transport is slow. They also cited the observation that a secreted form of GFP fails to form a gradient in wing discs [8] as evidence that efficient, free extracellular diffusion cannot occur, but this observation is more likely explained by the fact that GFP, with nothing to bind to, simply diffuses through and out of the wing disc so fast that no stable gradient can be formed. Finally, Schwank et al., [16] point to a growing body of literature suggesting that proteoglycans—glypicans in particular—control the formation of the Dpp gradient [11, 27, 28, 32–35], as evidence against transport by free extracellular diffusion.

The data presented here, however, lend no support to the idea of “proteoglycan-restricted” Dpp transport. Reversible binding of a large proportion of transported Dpp to glypicans (which, incidentally, are components of the cell surface, not the extracellular matrix) should have produced results in photoactivation and spatial FRAP experiments similar to those predicted by transcytosis models, and very different from what was observed (Fig. 2,3; see SI). Moreover, FRAP studies on dally mutant discs suggested that the proportion of mobile Dpp in the extracellular environment that is dally-bound is not particularly large (Fig. S3).

How can these results be reconciled with the growing body of literature suggesting an important role for proteoglycans in gradient formation, not only for Dpp, but many other morphogens [e.g. 11, 27, 28, 32–35, 36, 37–41]? To date, all experiments that have implicated proteoglycans in morphogen gradient formation have focused either on changes that occur in the distributions of total morphogen protein, or in morphogen activity (a function, presumably, of receptor occupancy). As discussed above, whenever transport occurs by free, rapid, extracellular diffusion, with only a small fraction of total morphogen being transported, the dynamics of the total and receptor-associated morphogen pools need not bear any relationship to transport rate. Rather, those dynamics will usually reflect processes downstream of and slower than transport, such as binding, internalization and degradation. It is, in fact, possible to attribute all known results of proteoglycan manipulation on morphogen gradient formation to effects on such downstream processes, especially given that proteoglycans not only bind morphogens, they influence the formation and stability of morphogen-receptor complexes [42].

Overall, the work presented here supports the simplest of models for morphogen transport: free diffusion in the extracellular space, hindered only by the viscosity of the extracellular fluid and the tortuosity of intercellular paths [43]. In some morphogen gradient systems, reversible binding to immobile molecules may also slow effective transport, but for Dpp in the wing disc no evidence of such an effect was obtained.

An important lesson to be gleaned from the present work is that morphogen gradients cannot generally be treated in the singular, as they are usually composites of coupled gradients in multiple compartments (e.g. free, surface-bound, intracellular, etc.). Even when they have similar steady-state shapes, such gradients can evolve very differently in time. For Dpp, the difference in dynamics between transported and stationary pools is evidently great, but this

may not always be so. In cases in which morphogen-receptor affinities are low (so that free extracellular concentrations need to be high), and there is little build-up of internalized morphogen receptor complexes, total morphogen dynamics might indeed reflect those of the molecules undergoing transport. The Fgf8 gradient of the zebrafish neural tube probably falls into this category, as large intracellular accumulations of morphogen are not seen in neural tube cells [17] and the affinity of Ffg8 for its receptors is notably weak (0.1–1 μM [44]). Not surprisingly, all observations of gradient dynamics in that system, whether by genetic manipulation, or direct measurement (e.g. FCS), have consistently supported a simple model of extracellular diffusion coupled to receptor-mediated uptake [17, 45].

EXPERIMENTAL PROCEDURES

Fly strains and transgenes

Flies were from Bloomington Drosophila Stock Center unless noted. DNA encoding Dendra2 was fused to Dpp and Wingless (Wg) using a strategy similar to that described for DppGFP and WgGFP [8, 46]: Dendra2 was cloned into an AvrII site introduced into Dpp between amino acids D485 and T486. Similarly, Dendra2 was inserted into an AvrII site introduced into Wg between W38 and W39. Both sequences were subcloned into pUAST, and transgenic flies generated by either P-element mediated transformation or PhiC31-mediated transformation [47]. UAS-DppGFP transgenic flies were previously described [8, 24]. Expression was driven using the dpp-gal4 driver. Quantitative imaging (see below) showed that Dpp-Dendra2 formed exponential gradients in the anterior and posterior compartments of the wing disc, with an average length scale of 21 + 1.5 μm in the posterior compartment. To assay for functional rescue by Dpp-Dendra2, Dpp^{d12}/CyO, Act-GFP; dpp-gal4/TM6B flies were crossed to dpp^{d14}/CyO, Act-GFP; UAS-DppDendra2. The dpp^{d12}/dpp^{d14}; dpp-gal4/UAS-DppDendra2 larvae were identified by lack of ubiquitous GFP and TM6B. The dpp^{d12}/dpp^{d14}; TM6B/UAS-DppDendra2 larvae served as a control.

Antibodies and immunostaining

Wing discs were fixed in 4% Formaldehyde for 15 min at room temperature, incubated with anti-spalt antibody (1:800; gift of Kavita Arora) at 4 °C overnight, and then Alexa 555-Goat anti rabbit (1:1000, Invitrogen) at room temperature for 1.5 hr.

Imaging

Wing discs were dissected from third instar larvae in M3 medium, and transferred to Clone-8 medium (Shields and Sang M3 [Sigma #S3652], with 10 μg/ml Insulin [Sigma #I9278], 2% heat-inactivated fetal bovine serum and 2.5% fly extract [48]) for time-lapse imaging. A channel was built on a glass slide with strips of magic tape (3M), filled with 60 μL Clone-8 medium, covered with a No. 1.5 cover slip (Corning), and sealed with rubber cement. Photobleaching and photoactivation were carried on a Fluoview1000 laser scanning confocal microscope (Olympus) with a 60×/1.2NA UPLSAPO water objective. DppDendra2 was excited with 488nm Argon laser, detected with a 505–540 band pass filter for the green channel and a 575–675 band pass filter for the red channel. The following settings were used for most imaging: 1% laser power for 488nm, 10% laser power for 558nm, 12 bit, photon counting mode, sequential scan mode, 2μs pixel dwell time, 1024 × 1024 pixels, 1.4 zoom, 0.147μm × 0.147 μm pixel size, 2.7 μm optical slice thickness. The machine was turned on 30 min before use, allowing the system to stabilize. During imaging, samples were maintained at 25 °C by a controller. Photobleaching was achieved with a 488nm laser at 100% power with a 100 μs pixel dwell time at seven z positions. Photoactivation was achieved using a 405 nm laser at 10% power and a 20μs pixel dwell time at single z position. During the chase period, the focal plane was maintained by a Zero-Drift Correction system (Olympus), and time points were taken at 5 minute intervals. At each time point, a stack of 5

overlapping (2.7 μm thick) optical sections was collected, each 1 μm apart from the next, covering the most apical part of the columnar cell layer of the disc.

Controls were carried out (Fig. S5) to demonstrate, under normal imaging conditions, a lack of significant photobleaching during imaging; a lack of dye saturation; a lack of detector saturation; and a linear relationship between Dendra2 concentration and fluorescence intensity. As in [9], controls also demonstrated that photobleaching occurred throughout the entire apicobasal depth of the wing disc (not shown).

Data analysis

Images were imported into ImageJ (NIH). Typically, a maximum projection of the z-stack was done at each time point. The mean intensity of an arbitrary region outside the wing disc was used as background, and subtracted from ROIs (regions of interest). For photobleaching, subtraction was also used to correct for bleach depth (incomplete bleaching). In photoactivation studies, it was often noticed that total fluorescence (summed over the entire image) was not constant over time, but in some cases underwent a gradual, linear increase (of up to 20% in rare cases) over the course of an hour. Control experiments suggested that this effect may have had to do with changes in disc thickness, or rearrangement of the locations of fluorescent puncta to more apical locations, which are detected more efficiently. Because of this effect, photoactivation data were typically analyzed after normalization to total red fluorescence of the entire imaged area (or of a subregion of the imaged area containing most of the red signal).

Fluorescence correlation spectroscopy and Pair Correlation Function microscopy

For FCS, wing discs were mounted in Ringer solution to minimize autofluorescence. Single point FCS was performed using either a Zeiss LSM510 Meta and Confocor3 system with a C-Apochromat 40×/1.20 NA water immersion objective or a Zeiss LSM710 system with a C-Apochromat 63×/1.20 NA water immersion objective. Measurements were performed in the apical part of the disc at room temperature. Each Confocor3 measurement lasted 100 sec. Each LSM710 measurement lasted about 75 sec. Normally ten different locations were measured for each disc. Pixels were subjected to a 1-second pre-bleach at 100% laser power just prior to each measurement, to reduce contributions from immobile fluorophores. Data were analyzed with Confocor3 software or SimFCS (Laboratory for Fluorescence Dynamics, UC Irvine). Pair Correlation Function microscopy (pCF) was done with the SimFCS software and the LSM710 system. Data were collected using the line scan mode with pixel size 105 nm, pixel dwell time 6.3 μs, line time 471 μs, and 100,000 lines with 32 pixels per line.

Use of pre-photobleaching to suppress immobile background due to a slowly-recovering pool

As reported by Kicheva et al., [9] for DppGFP, and confirmed here for DppDendra2 (Fig. S1), recovery of Dpp fluorescence after photobleaching plateaus within the first hour at about 15– 30% of initial fluorescence. The existence of a large non-recovering background (“immobile fraction”) potentially reduces the sensitivity with which one can follow the dynamics of changes in fluorescence. In some experiments (Fig. S1–S2), we lowered this background by pre-photobleaching a large region, then waiting 30 min for recovery (long enough for substantial return of the rapidly-recovering fluorescence). As shown in Fig. S1, under these conditions, the “mobile fraction” of Dpp fluorescence rises to about 75%. The fact that it does not rise to 100% indicates that original “immobile fraction” is not truly a static pool, but simply one that recovers on a slow time scale. As described elsewhere (SI), this behavior can be modeled by assuming that some internalized Dpp becomes transferred to a pool that degrades only very slowly (e.g. a long-lived vesicular compartment).

Numerical solutions to differential equations

Systems of partial differential equations were solved using *Mathematica* software (Wolfram Research).

Highlights

1. We identify methodological errors in the estimation of morphogen transport that have led to the view that some morphogens, such as decapentaplegic (Dpp), spread by inherently slow processes such as planar transcytosis or “restricted” diffusion.
2. We utilize a combination of short- and long-time scale methods to show that the spreading of Dpp in the fruitfly wing disc occurs by simple, free diffusion in the extracellular space
3. We present mathematical analysis that elucidates the circumstances under which innacurate estimates of morphogen transport can be obtained from fluorescence recovery-based methods, such as FRAP.

Supplementary Material

Refer to Web version on PubMed Central for supplementary material.

Acknowledgments

We thank Kavita Arora for helpful advice. Supported by NIH grants GM067247 and GM076516

References

1. Crick FHC. Diffusion in Embryogenesis. Nature. 1970; 225:420–422. [PubMed: 5411117]
2. Lander AD, Nie Q, Wan FY. Do morphogen gradients arise by diffusion? Dev Cell. 2002; 2:785–796. [PubMed: 12062090]
3. Eldar A, Dorfman R, Weiss D, Ashe H, Shilo BZ, Barkai N. Robustness of the BMP morphogen gradient in *Drosophila* embryonic patterning. Nature. 2002; 419:304–308. [PubMed: 12239569]
4. Eldar A, Rosin D, Shilo BZ, Barkai N. Self-enhanced ligand degradation underlies robustness of morphogen gradients. Dev Cell. 2003; 5:635–646. [PubMed: 14536064]
5. Mizutani CM, Nie Q, Wan FY, Zhang YT, Vilmos P, Sousa-Neves R, Bier E, Marsh JL, Lander AD. Formation of the BMP activity gradient in the Drosophila embryo. Dev Cell. 2005; 8:915–924. [PubMed: 15935780]
6. White RJ, Nie Q, Lander AD, Schilling TF. Complex regulation of cyp26a1 creates a robust retinoic acid gradient in the zebrafish embryo. PLoS Biol. 2007; 5:e304. [PubMed: 18031199]
7. Nahmad M, Stathopoulos A. Dynamic interpretation of hedgehog signaling in the Drosophila wing disc. PLoS Biol. 2009; 7:e1000202. [PubMed: 19787036]
8. Entchev EV, Schwabedissen A, Gonzalez-Gaitan M. Gradient formation of the TGF-beta homolog Dpp. Cell. 2000; 103:981–991. [PubMed: 11136982]
9. Kicheva A, Pantazis P, Bollenbach T, Kalaidzidis Y, Bittig T, Julicher F, Gonzalez-Gaitan M. Kinetics of morphogen gradient formation. Science. 2007; 315:521–525. [PubMed: 17255514]
10. Kruse K, Pantazis P, Bollenbach T, Julicher F, Gonzalez-Gaitan M. Dpp gradient formation by dynamin-dependent endocytosis: receptor trafficking and the diffusion model. Development. 2004; 131:4843–4856. [PubMed: 15358671]
11. Belenkaya TY, Han C, Yan D, Opoka RJ, Khodoun M, Liu H, Lin X. Drosophila Dpp morphogen movement is independent of dynamin-mediated endocytosis but regulated by the glypican members of heparan sulfate proteoglycans. Cell. 2004; 119:231–244. [PubMed: 15479640]

12. Bollenbach T, Kruse K, Pantazis P, Gonzalez-Gaitan M, Julicher F. Morphogen transport in epithelia. Phys Rev E Stat Nonlin Soft Matter Phys. 2007; 75:011901. [PubMed: 17358178]
13. Wolpert L. Diffusible gradients are out - an interview with Lewis Wolpert. Interviewed by Richardson, Michael K. Int J Dev Biol. 2009; 53:659–662. [PubMed: 19557674]
14. Hsiung F, Ramirez-Weber FA, Iwaki DD, Kornberg TB. Dependence of Drosophila wing imaginal disc cytonemes on Decapentaplegic. Nature. 2005; 437:560–563. [PubMed: 16177792]
15. Ramirez-Weber FA, Kornberg TB. Cytonemes: cellular processes that project to the principal signaling center in Drosophila imaginal discs. Cell. 1999; 97:599–607. [PubMed: 10367889]
16. Schwank G, Dalessi S, Yang SF, Yagi R, de Lachapelle AM, Affolter M, Bergmann S, Basler K. Formation of the long range Dpp morphogen gradient. PLoS Biol. 2011; 9:e1001111. [PubMed: 21814489]
17. Yu SR, Burkhardt M, Nowak M, Ries J, Petrasek Z, Scholpp S, Schwille P, Brand M. Fgf8 morphogen gradient forms by a source-sink mechanism with freely diffusing molecules. Nature. 2009; 461:533–536. [PubMed: 19741606]
18. Gregor T, Wieschaus EF, McGregor AP, Bialek W, Tank DW. Stability and nuclear dynamics of the bicoid morphogen gradient. Cell. 2007; 130:141–152. [PubMed: 17632061]
19. Abu-Arish A, Porcher A, Czerwonka A, Dostatni N, Fradin C. High mobility of bicoid captured by fluorescence correlation spectroscopy: implication for the rapid establishment of its gradient. Biophys J. 2010; 99:L33–L35. [PubMed: 20712981]
20. Castle BT, Howard SA, Odde DJ. Assessment of Transport Mechanisms Underlying the Bicoid Morphogen Gradient. Cell Mol Bioeng. 2011; 4:116–121. [PubMed: 21892361]
21. Schier AF, Needleman D. Developmental biology: Rise of the source-sink model. Nature. 2009; 461:480–481. [PubMed: 19779439]
22. Porcher A, Dostatni N. The bicoid morphogen system. Curr Biol. 2010; 20:R249–R254. [PubMed: 20219179]
23. Bollenbach T, Pantazis P, Kicheva A, Bokel C, Gonzalez-Gaitan M, Julicher F. Precision of the Dpp gradient. Development. 2008; 135:1137–1146. [PubMed: 18296653]
24. Teleman AA, Cohen SM. Dpp gradient formation in the Drosophila wing imaginal disc. Cell. 2000; 103:971–980. [PubMed: 11136981]
25. Lippincott-Schwartz J, Altan-Bonnet N, Patterson GH. Photobleaching and photoactivation: following protein dynamics in living cells. Nat Cell Biol. 2003; (Suppl):S7–S14. [PubMed: 14562845]
26. Gurskaya NG, Verkhusha VV, Shcheglov AS, Staroverov DB, Chepurnykh TV, Fradkov AF, Lukyanov S, Lukyanov KA. Engineering of a monomeric green-to-red photoactivatable fluorescent protein induced by blue light. Nat Biotechnol. 2006; 24:461–465. [PubMed: 16550175]
27. Akiyama T, Kamimura K, Firkus C, Takeo S, Shimmi O, Nakato H. Dally regulates Dpp morphogen gradient formation by stabilizing Dpp on the cell surface. Dev Biol. 2008; 313:408–419. [PubMed: 18054902]
28. Fujise M, Takeo S, Kamimura K, Matsuo T, Aigaki T, Izumi S, Nakato H. Dally regulates Dpp morphogen gradient formation in the Drosophila wing. Development. 2003; 130:1515–1522. [PubMed: 12620978]
29. Hinde E, Cardarelli F, Digman MA, Gratton E. In vivo pair correlation analysis of EGFP intranuclear diffusion reveals DNA-dependent molecular flow. Proc Natl Acad Sci U S A. 2010
30. Cardarelli F, Gratton E. In vivo imaging of single-molecule translocation through nuclear pore complexes by pair correlation functions. PLoS One. 2010; 5:e10475. [PubMed: 20454622]
31. Digman MA, Gratton E. Imaging barriers to diffusion by pair correlation functions. Biophys J. 2009; 97:665–673. [PubMed: 19619481]
32. Han C, Belenkaya TY, Khodoun M, Tauchi M, Lin X. Distinct and collaborative roles of Drosophila EXT family proteins in morphogen signalling and gradient formation. Development. 2004; 131:1563–1575. [PubMed: 14998928]
33. Takei Y, Ozawa Y, Sato M, Watanabe A, Tabata T. Three Drosophila EXT genes shape morphogen gradients through synthesis of heparan sulfate proteoglycans. Development. 2004; 131:73–82. [PubMed: 14645127]

34. Bornemann DJ, Duncan JE, Staatz W, Selleck S, Warrior R. Abrogation of heparan sulfate synthesis in Drosophila disrupts the Wingless, Hedgehog and Decapentaplegic signaling pathways. Development. 2004; 131:1927–1938. [PubMed: 15056609]
35. Crickmore MA, Mann RS. Hox control of morphogen mobility and organ development through regulation of glypican expression. Development. 2007; 134:327–334. [PubMed: 17166918]
36. Ohkawara B, Iemura S, ten Dijke P, Ueno N. Action range of BMP is defined by its N-terminal basic amino acid core. Curr Biol. 2002; 12:205–209. [PubMed: 11839272]
37. Han C, Belenkaya TY, Wang B, Lin X. Drosophila glypicans control the cell-to-cell movement of Hedgehog by a dynamin-independent process. Development. 2004; 131:601–611. [PubMed: 14729575]
38. Han C, Yan D, Belenkaya TY, Lin X. Drosophila glypicans Dally and Dally-like shape the extracellular Wingless morphogen gradient in the wing disc. Development. 2005; 132:667–679. [PubMed: 15647319]
39. Gallet A, Staccini-Lavenant L, Therond PP. Cellular trafficking of the glypican Dally-like is required for full-strength Hedgehog signaling and wingless transcytosis. Dev Cell. 2008; 14:712–725. [PubMed: 18477454]
40. Yan D, Lin X. Shaping morphogen gradients by proteoglycans. Cold Spring Harb Perspect Biol. 2009; 1:a002493. [PubMed: 20066107]
41. Umulis D, O'Connor MB, Blair SS. The extracellular regulation of bone morphogenetic protein signaling. Development. 2009; 136:3715–3728. [PubMed: 19855014]
42. Kuo WJ, Digman MA, Lander AD. Heparan sulfate acts as a bone morphogenetic protein coreceptor by facilitating ligand-induced receptor hetero- oligomerization. Mol Biol Cell. 2010; 21:4028–4041. [PubMed: 20861306]
43. Rusakov DA, Kullmann DM. Geometric and viscous components of the tortuosity of the extracellular space in the brain. Proc Natl Acad Sci U S A. 1998; 95:8975–8980. [PubMed: 9671789]
44. Olsen SK, Li JY, Bromleigh C, Eliseenkova AV, Ibrahimi OA, Lao Z, Zhang F, Linhardt RJ, Joyner AL, Mohammadi M. Structural basis by which alternative splicing modulates the organizer activity of FGF8 in the brain. Genes Dev. 2006; 20:185–198. [PubMed: 16384934]
45. Scholpp S, Brand M. Endocytosis controls spreading and effective signaling range of Fgf8 protein. Curr Biol. 2004; 14:1834–1841. [PubMed: 15498491]
46. Pfeiffer S, Ricardo S, Manneville JB, Alexandre C, Vincent JP. Producing cells retain and recycle Wingless in Drosophila embryos. Curr Biol. 2002; 12:957–962. [PubMed: 12062063]
47. Bischof J, Maeda RK, Hediger M, Karch F, Basler K. An optimized transgenesis system for Drosophila using germ-line-specific phiC31 integrases. Proc Natl Acad Sci U S A. 2007; 104:3312–3317. [PubMed: 17360644]
48. Cullen CF, Milner MJ. Parameters of growth in primary cultures and cell lines established from Drosophila imaginal discs. Tissue Cell. 1991; 23:29–39. [PubMed: 1905427]

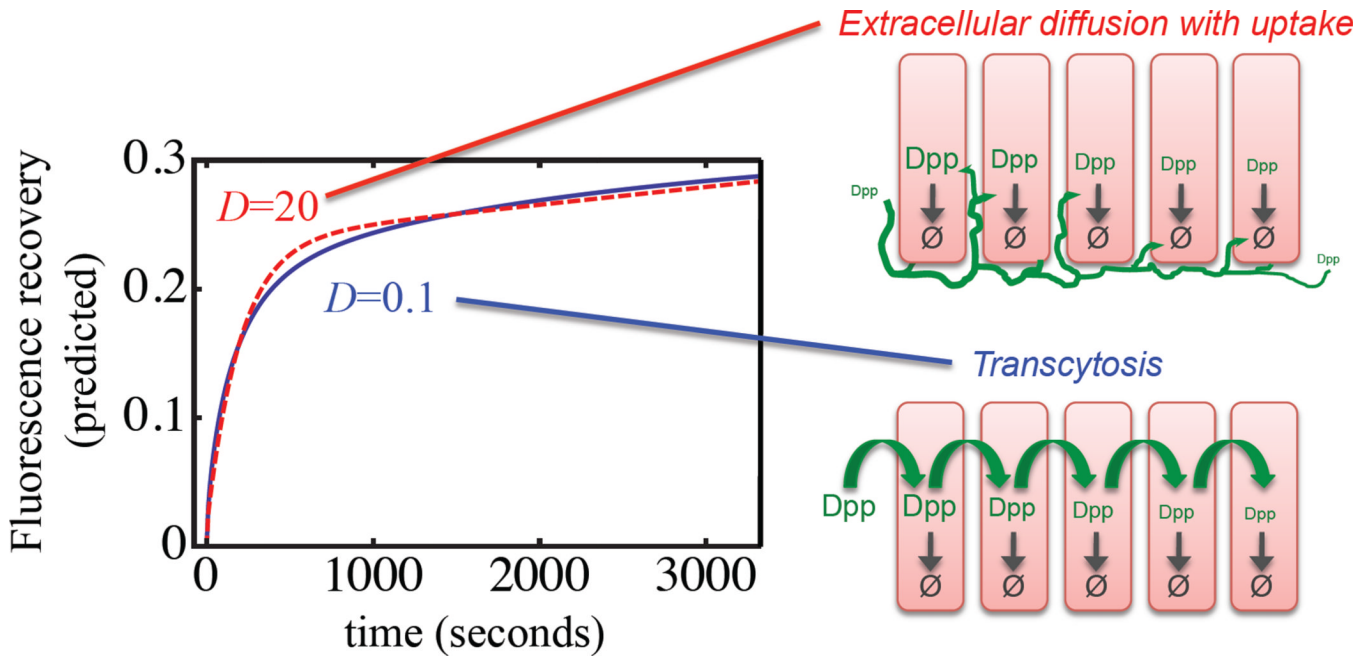

Fig. 1. Fluorescence recovery after photobleaching (FRAP) can provide little or no information about transport

In models of morphogen transport by extracellular diffusion with cellular uptake, accumulation, and degradation, if diffusion is fast enough, overall FRAP kinetics will tend to reflect the time scale of degradation, not transport. This is illustrated by simulating the expected results of FRAP within a 10 μm-wide stripe adjacent to the source of the morphogen Dpp in the *Drosophila* wing disc according either to a model of transcytotic transport (blue) with an effective diffusion coefficient of 0.1 $\mu m^2\ sec^{-1}$ [9], or a model based on free extracellular diffusion with uptake (red, dashed), with a diffusion coefficient of 20 $\mu m^2\ sec^{-1}$. For further details, see SI.

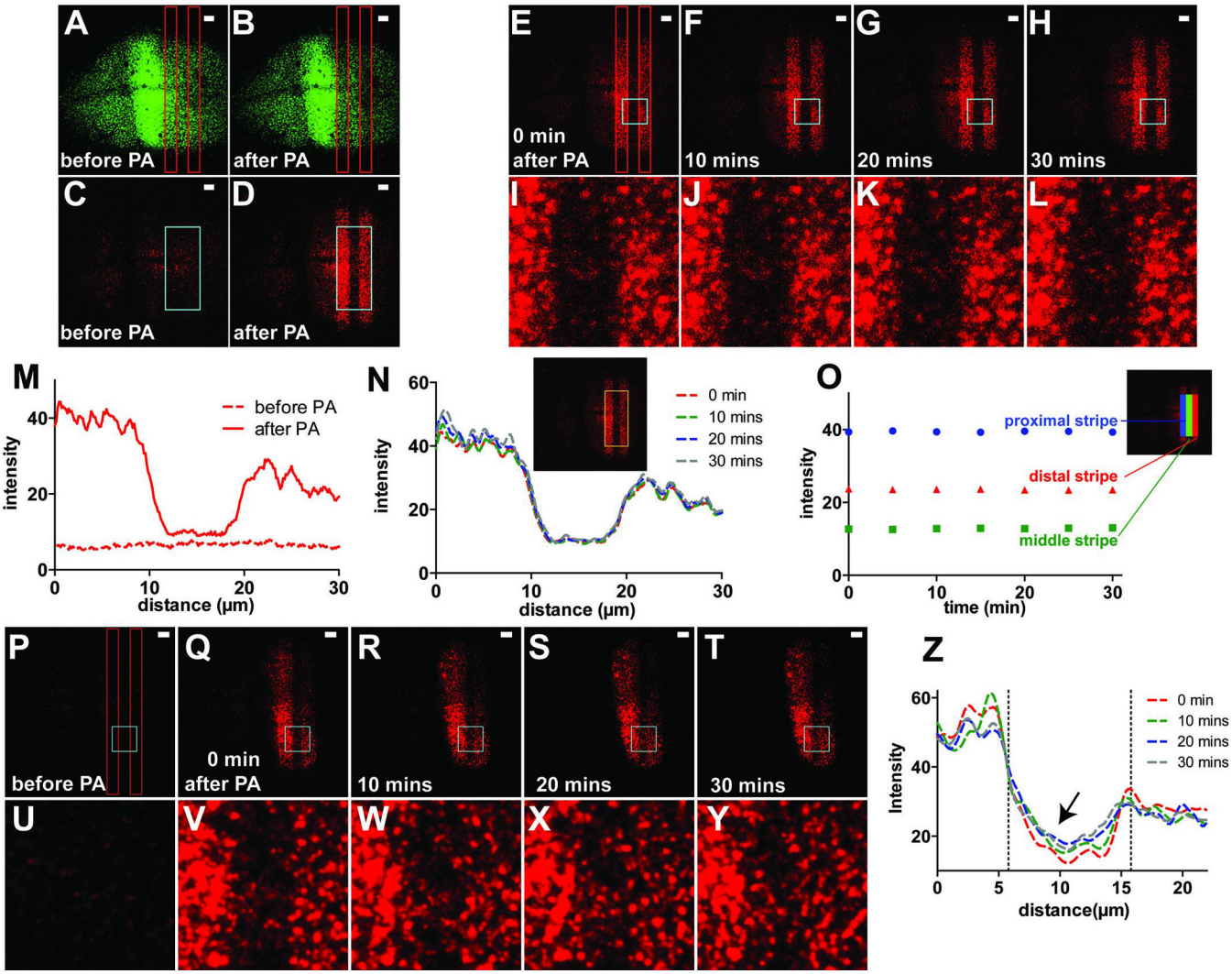

Fig. 2. Lack of spreading of photoactivated DppDendra2

(A-D) Confocal images of a DppDendra2-expressing wing disc before and after photoactivation (PA). Before PA, bilaterial exponential gradients are observed along the horizontal (anteroposterior axis) in the green channel (A) with minimal red signal (C). PA was carried out in two rectangular regions (red boxes in A, B) using a 20 μsec pulse of 405 nm light, producing two red fluorescent stripes (D). **(E-H)** Images after PA. Five optical slices covering the apical part of the disc were taken at 5-minute intervals for 30 min, maximum-projected, and intensity profiles calculated (similar results were obtained when optical slices were summed, instead of maximum-projected). Cyan boxes in E-H are magnified in I-L. **(M)** Average intensity along the vertical (dorsoventral axis) is plotted along the horizontal axis of the cyan box in C and D. **(N)** Intensity profiles along the horizontal axis of the yellow box (see inset) at times after PA. **(O)** Average intensities inside the proximal (near the morphogen source) and distal PA-stripes, and the region lying between them ("middle stripe"), at different times. The proximal, middle and distal stripes correspond to the blue, green and red regions in the inset. **(P-Z)** Spreading of photoactivated WinglessDendra2. Panels P-T are time-lapse images from a wing disc expressing WinglessDendra2 in the Dpp domain (dpp-gal4/UAS-WinglessDendra2) and photoactivated and imaged as in A-D. (**U-Y**) Magnified views of the cyan boxes in P-T. **(Z)** Intensity

profiles along the horizontal axis of each cyan box were plotted at different time points. Dashed lines mark the boundaries of the two photoactivated regions. Note significant spreading of fluorescence (arrow). In addition, in Dpp-Dendra2-expressing discs in which the entire disc (including the production region) was photoactivated, except for a small stripe, we also observed some spreading of fluorescence into the non-photoactivated region (data not shown). Bars in A-H, P-T = 10 μm.

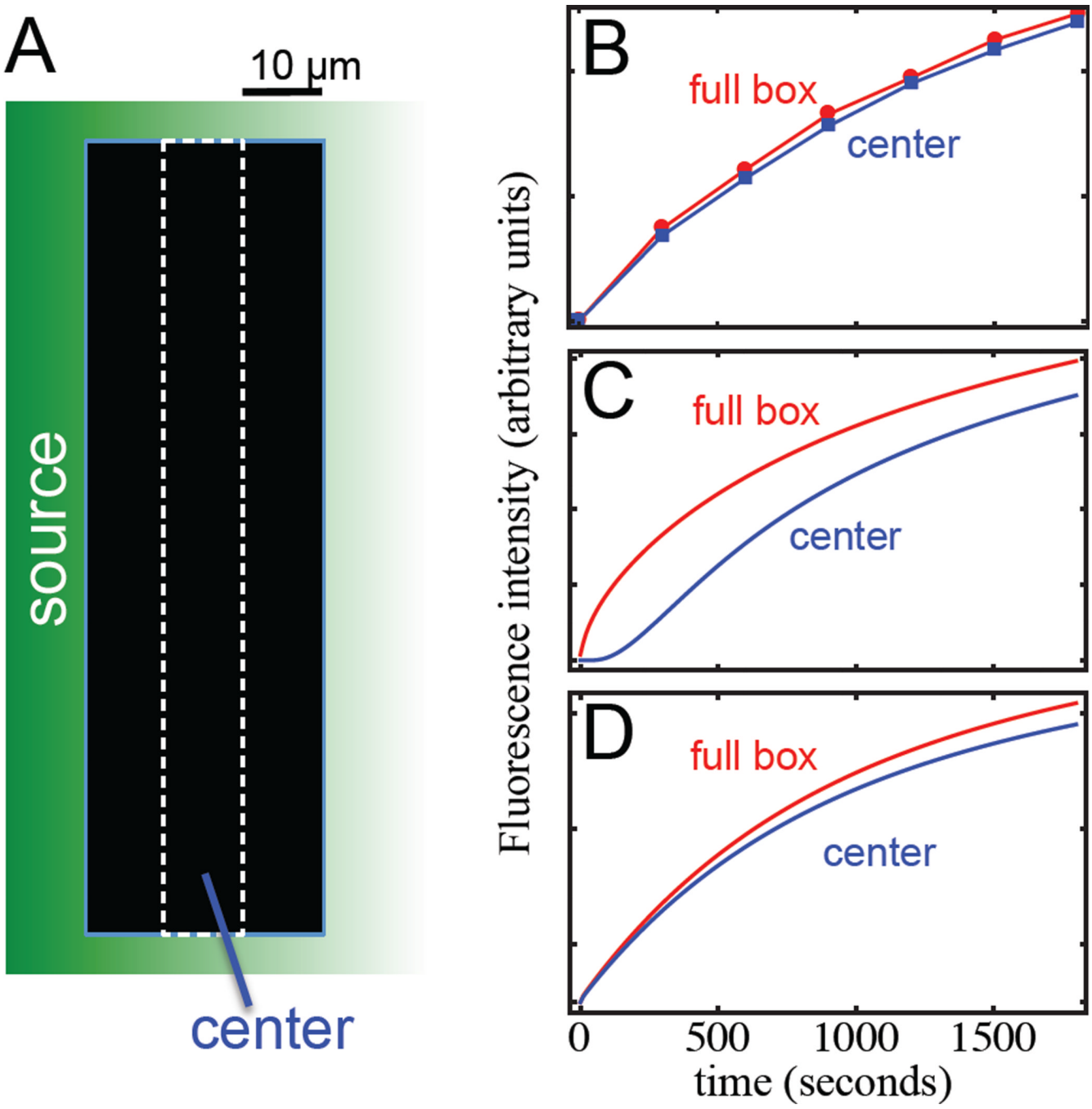

Fig. 3. Results of "spatial" FRAP support transport by rapid diffusion

Whereas the kinetics of FRAP within a single photobleached region cannot necessarily distinguish between slow and fast transport (see Fig. 1), it should be possible to do so by comparing FRAP kinetics at different locations within a photobleached region. As diagrammed in (**A**), a 30 × 150 μm wide rectangle was photobleached in the posterior compartment of a DppDendra2-expressing wing disc and observed at multiple locations for 30 min. Fluorescence intensities, corrected for bleach depth, were measured for the entire box, as well as for a 10 × 150 μm region in the center of the box. The results of a typical experiment are shown in (**B**). The predictions of models based on transcytosis (D=0.1 μm^2

sec^{-1}) and free extracellular diffusion (D= 20 μm^2 sec^{-1}) are shown in (**C**) and (**D**), respectively. Note the significant time displacement (~250 sec) between the two curves required by the transcytosis model (C; similar behavior would be produced by slow, "restricted extracellular diffusion"). The delay corresponds to the time required for a molecule with D=0.1 μm^2 sec^{-1} to travel 10 μm.

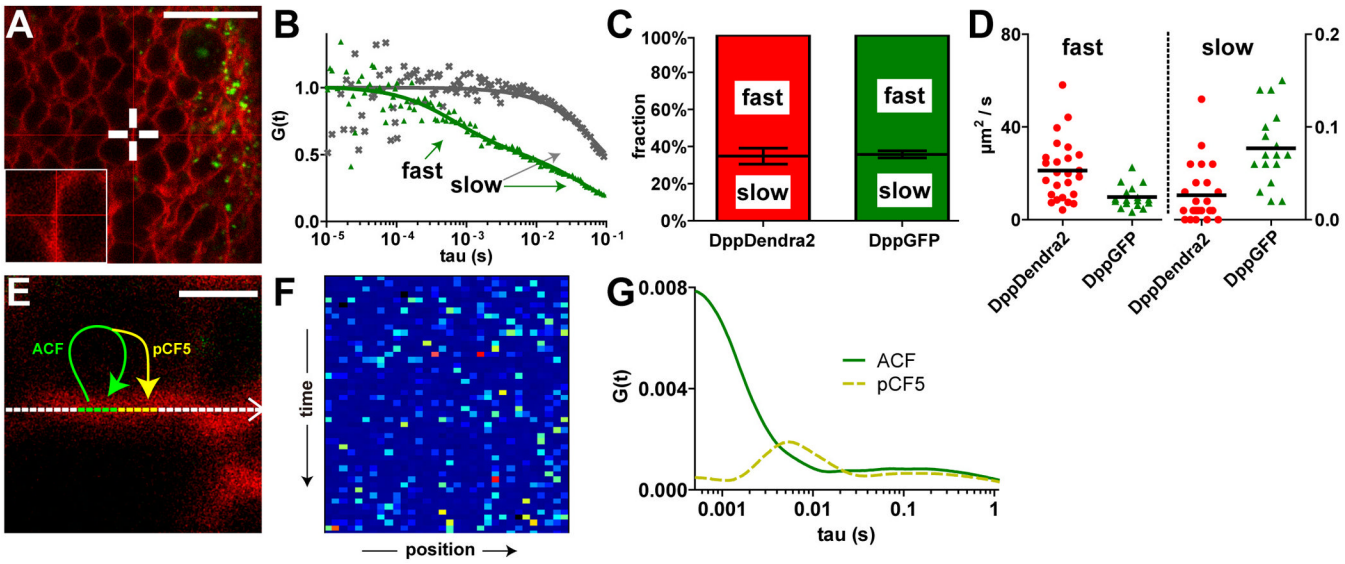

Fig. 4. Measuring extracellular diffusion of Dpp

(A) Confocal images of DppDendra2-expressing wing discs used for FCS. Green: DppDendra2; red: FM4-64 (to label cell membranes). Cross hairs mark location of FCS measurement. Inset shows a magnified view. Bar=10 μm. **(B)** Autocorrelation curves for DppDendra2 (green) and a membrane-anchored control, cd8GFP (grey; expressed under the control of dpp-Gal4). Data from DppDendra2 fit a two-component diffusion model with fast and slow components. **(C)** Proportions of molecules in fast and slow pools measured for DppDendra2 (as in B) and DppGFP (not shown). **(D)** Caclulated diffusion coefficients. Each point represents an independent measurement at a different location in a total of 11 wing discs for DppDendra2 and 4 wing discs for DppGFP. Averages (black bars) were 21 ± 3 $\mu m^2\ sec^{-1}$ and 0.03 ± 0.006 $\mu m^2\ sec^{-1}$ for DppDendra2, and 10 ± 1 $\mu m^2\ sec^{-1}$ and 0.08 ± 0.01 $\mu m^2\ sec^{-1}$ for DppGFP (values are means ± SEM). **(E)** Pair correlation function (pCF) microscopy was carried out by repeatedly scanning a 3.2 μm-long line along a site of cell contact in a DppDendra2-expressing disc (stained as in A). Bar=1μm. Fluorescence intensities were converted to an intensity carpet **(F)**, in which the horizontal and vertical directions represent position and time, respectively, and intensity is color-coded. Autocorrelation, calculated at each location and averaged over all locations was plotted ("ACF") in (**G**). For pair correlation, fluctuations in each of five pixels (depicted in green along the line in E) were each cross-correlated with pixels 5 positions to the right (depicted in yellow in E), and the correlation curves averaged and plotted ("pCF5"). The position of the peak in the pCF5 curve corresponds to the average time delay required for DppDendra2 to move 5 pixels.